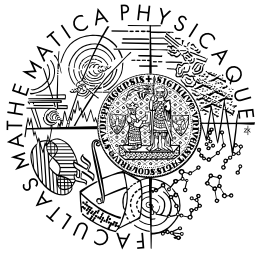

FACULTY
OF MATHEMATICS
AND PHYSICS
Charles University

Macromolecules and nanostructures in a low-temperature plasma

Habilitation Thesis

Jaroslav Kousal

Prague 2022

Acknowledgements

I thank all the colleagues, too numerous to name, that have helped me during the previous years of my carrier. I also thank my family and friends for their support during all this time. I would like to express a special thanks to professor Hynek Biederman, who played a pivotal role in drawing my interest to plasma-based deposition techniques and to the field of plasma polymers in particular.

Contents

1. Preface

Dear reader,

the author of this thesis had a hard time selecting one of the sub-topics of his work to describe. Ultimately, he realized that they are too connected to each other to be fully separated.

In this habilitation thesis, the selected author's publications will be used to highlight the connections of the processes during plasma-surface interaction [JK1, JK2, JK3], processes of formation of nanoparticles and nanocomposites [JK4, JK5, JK6, JK7] and a new view on the plasma polymers [JK8, JK9, JK10, JK11, JK12].

Brief commentaries to these publications regarding motivations, geneses, and highlighted outputs together with a broader overview will be given. For the context, selected illustrative examples from the related research fields will be referenced, with some emphasis on works where the author of this thesis was also involved.

Jaroslav Kousal, 2022

2. Macromolecules and nanostructures in a low-temperature plasma

2.1 Plasma-surface interactions

2.1.1 Low-temperature plasma

Plasma, in the most concise way, can be regarded as a "medium containing free charged particles that exhibits a 'collective behaviour'". Even in cases when the charged particles represent only a small minority of the matter in a plasma, the long-distance character of the electromagnetic interactions (both from externally and internally generated fields) gives plasma many properties unusual in the non-ionized matter.

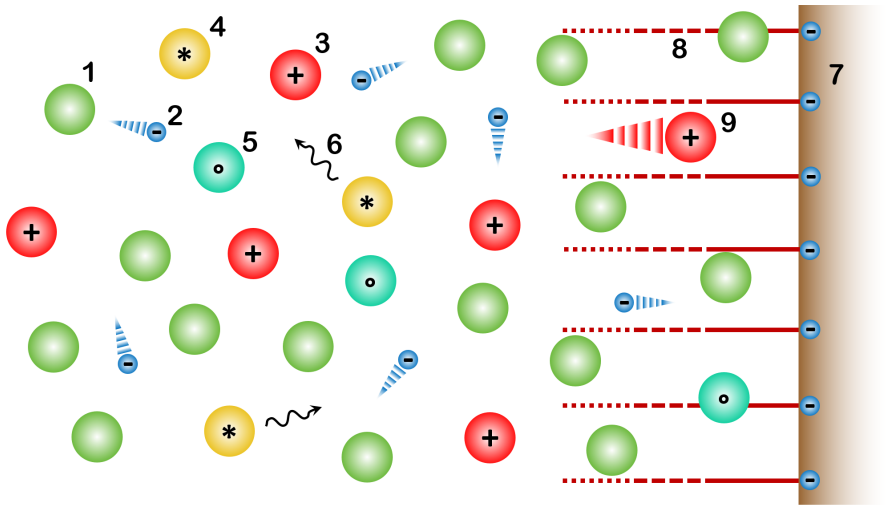

Figure 2.1: Schematic representation of non-magnetized low-temperature plasma. 1–neutral gas; 2–electrons; 3–ions; 4–excited species; 5–radicals; 6–photons; 7–wall/substrate; 8–electric field near the wall (sheath); 9–fast ion.

Low-temperature plasma is typically a non-equilibrium environment consisting of "cold" neutral gas (T_n <0.1 eV), ions and light and "hot" energetic electrons (T_e >1 eV), together with other species originating mostly from the neutral gas (Fig. 2.1). The energies in the "hot" particles' energy distribution reach the threshold for the dissociation of atomic bonds while most of the molecules, if present, can remain below the temperature of their thermal decomposition. In this way, this thermodynamic non-equilibrium

promotes additional reaction pathways not known from classical chemistry [1]. For most processes in the low-temperature plasma, the concentration of electrons (plasma density) and electron temperature (energy distribution) are the key parameters. Additionally, local electromagnetic fields can also accelerate charged particles to considerable energies. These effects are the basis of utilizing of low-temperature plasma as a tool to modify (section 2.1.2) and/or synthesize (sections 2.1.3, 2.2.1, 2.2.2, 2.3) condensed matter. For an overview of the theory and applications of low-temperature plasma, refer e.g. to [2].

2.1.2 Plasma surface treatment

When low-temperature plasma interacts with adjacent surfaces, the higher mobility of electrons causes charging of the surface of an electrically floating object in a plasma to be negatively charged. This charging forms a layer with non-zero electric field intensity (”sheath”) near the surface that accelerates ions (which are mostly positively charged) toward the surface. Under most conditions, the ion energy ($\sim$ few eV) is too low to directly influence the interatomic bonds in the material of the surface unless the potential difference in the sheath is increased externally, e.g. at the powered cathode in the discharge (section 2.1.3).

However, it is important to note that during the plasma-surface interaction, the excess energy is transferred in significant part into heat. If the local temperature of the surface of the treated material becomes comparable to its melting point, the material ablation rate increases significantly [3]. For polymers, this temperature threshold is at relatively low temperatures, typically just a few hundred K above room temperature.

Plasma surface treatment already has industrially well-established applications [4], like wettability and roughness control or a plasma cleaning, including cleaning the surfaces from organic contaminants like proteins. This is especially important in the field of biomedicine since proteins can be biologically active (or can even, in the case of prions, represent infectious agens themselves) and some proteins are resistant to classical sterilization procedures [5]. Removal of such contaminants via plasma treatment falls within the topic of ”plasma sterilization”, itself being a part of the broader field of so-called ”plasma medicine” (a recent review can be found in [6]).

To represent the effects of plasma on a ”fragile” matter of proteins, bovine-serum albumin (BSA), generally one of the common ”model” proteins, was chosen [JK1]. In such case, even so-called afterglow (decaying, cold, non-

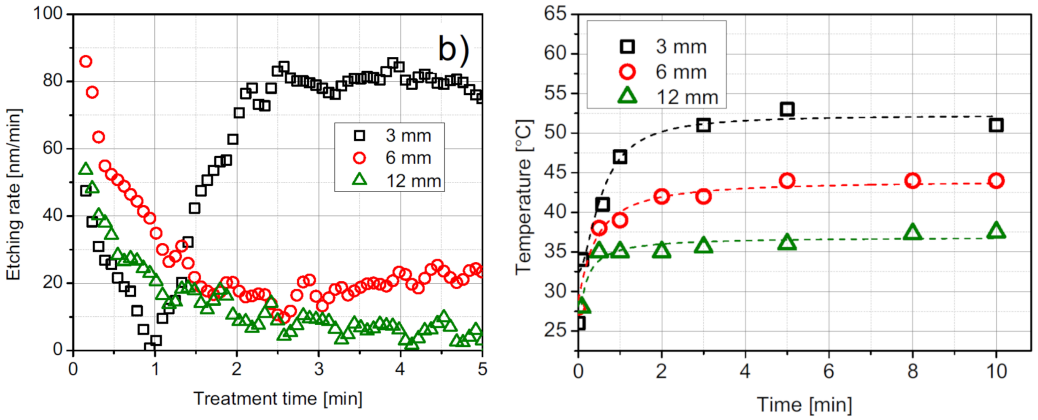

Figure 2.2: Etching of thin BSA film by a plasma jet in dependence on the nozzle-sample distance. Left: Etching rate vs time. Right: Sample temperature vs time. Reproduced from [JK1].

active) plasma blown out of the low-temperature plasma jet at atmospheric pressure was sufficient to etch the BSA film. The modification of the surface of the film progressed mostly in the first 10–20% of the thickness of the film, where a layer of oxidized, more etching-resistant material was formed. It was demonstrated that even temperatures just above 40 °C led to an significant increase of the material ablation rate (Fig. 2.2). Qualitatively similar effects were also observed in magnetron sputtering of polymers (section 2.1.3).

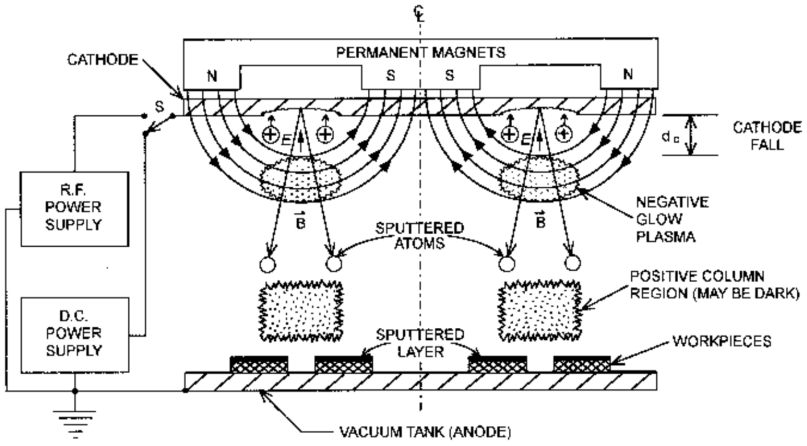

Figure 2.3: Scheme of a planar magnetron. Reproduced from [7].

2.1.3 Magnetron sputtering

Thin films prepared by sputtering of materials in plasma were already observed in the early discharge tubes. With the invention of magnetron sputtering in the 1930s, one of the most widely used vacuum-based techniques for thin film preparation was born [8].

In magnetron (in the meaning of a sputtering device), a partially magnetically trapped low-temperature plasma ring is formed above a negatively charged electrode covered with a material that serves as a target for ion bombardment (Fig. 2.3). Electrons are held above the cathode by the combination of orbiting the magnetic field lines, the effect of the magnetic mirror and the $E \times B$ drift. Ions from the bulk of the plasma are accelerated through an electric field in a sheath layer towards the surface of the magnetron target into the so-called erosion zone (erosion track). These ions gain an energy of higher tens to hundreds eV. At such impact energies, both elastic and inelastic collisions of the impacting ions with the atoms of the target occur. Since the incoming atom has sufficient excess kinetic energy, the impacted atom itself can gain energy sufficient to displace another atom. In this way, a collisional avalanche in the target material occurs, leading to the expulsion (sputtering) of ~ 1 atom of the target material per 1 incoming ion. Target atoms typically leave the material in a neutral state so they can easily come through the plasma via diffusion and they can be deposited on the substrate, producing a thin film.

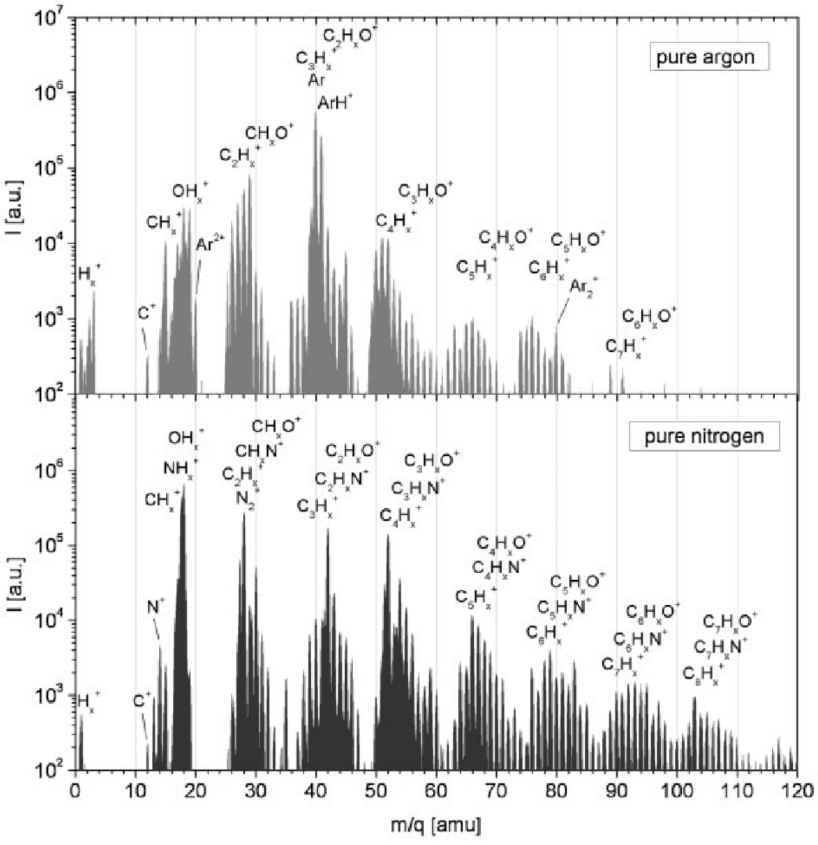

Figure 2.4: Positive ion mass spectra near the substrate plane during sputtering of polypropylene in Ar (up) and N_2 (down). Reproduced from [JK2].

More commonly, the surface of the target is supposed to be conductive (to prevent charge accumulation). However, it is possible to sputter insulat-

ing materials using high-frequency (∼MHz, radio frequency, RF) plasma. The first experiments with the sputtering of polymers were reported at the end of the 1960s [9], with initial interest especially in fluorocarbon polymers [10]. The founder of the author's group, prof. Hynek Biederman, is one of the pioneers of the magnetron sputtering of polymers [11, 12, 13]. Therefore, the author's group frequently utilizes the know-how in this sub-field of so-called plasma polymerization (section 2.3). The typical molecular structure of material prepared by the sputtering of polymers is highly irregular and nearly fully crosslinked since the sputtered fragments – the building blocks – are very short (few atoms). However, this is not a drawback in many cases, especially when properties like (non)conductivity, hardness or uniformity are more important than the exact polymer chain structure. In many cases, the functionality of the film is dependent basically just on the composition of the surface. Then even a thin (∼20 nm) film can e.g. make an efficient binding layer between two otherwise poorly adhering materials [14, 15].

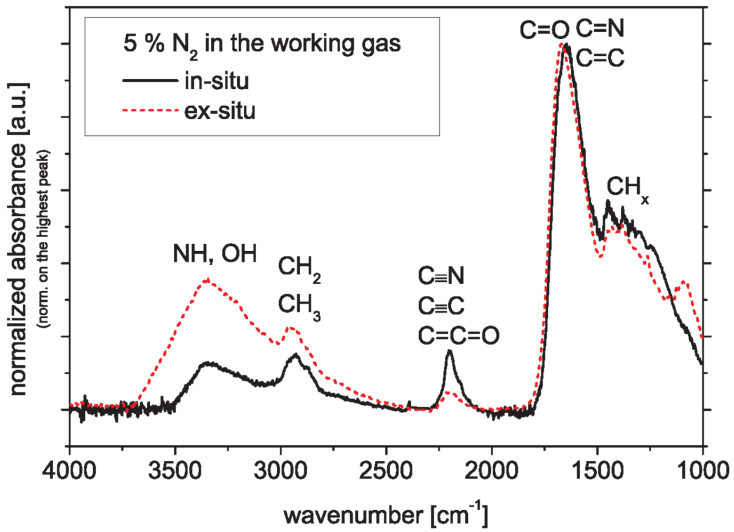

Figure 2.5: Comparison of infrared spectra of the as-deposited film prepared by sputtering of nylon (measured in–situ) and of the same film measured ex-situ after the exposure to ambient air. The peak near 3300 cm^{-1} shows the absorption of –OH groups and the shift of the peak near 1650 cm^{-1} shows the replacement of C=N groups with C=O groups. Reproduced from [JK3].

Based on the existing knowledge on the binding of polar groups and especially the amino groups to proteins, films with high content of –NH and/or $–NH_2$ groups ("amino-rich coatings") were considered a "hot topic", especially in the 2000s. Motivated by the potential biomedical applications, various approaches to prepare amino–rich (and nitrogen-rich in general) surfaces were explored, including plasma polymerization and plasma grafting [16, 17, 18].

The sputtering of polymers is well suited for the preparation of films for

these "interfacial" applications. There are two basic ways how to make a thin film with desired functional chemical groups – either sputter a polymer in a reactive gas mixture that promotes forming of such groups or sputter a polymer already containing these groups.

The first approach was performed in [JK2], where polypropylene was sputtered in Ar–N_2 mixtures. As expected, nitrogen was incorporated in the films, as well as on their surfaces, as was demonstrated by the films' wettability. Additionally, a big increase in the deposition rate with the increasing amount of N_2 was found. This can be explained by the formation of shorter and more volatile polymer chains on the surface of the polymer target via the passivation of temporary radicals by nitrogen. Shorter polymer chains are then more readily sputtered or just thermally released from the target.

The former effect paradoxically leads to the presence of a heavier molecular species in the plasma during sputtering in N_2 than in Ar. This is visible in Fig. 2.4. A slight shift of the "carbon fingers" in the mass spectra by $\sim$2 amu shows the presence of nitrogen bound in the sputtered polymer fragments.

The latter effect was also clearly observed during sputtering at higher magnetron powers, where also additional thermal scission of the polymer chains on the surface of the target takes place. This corresponds well with the findings of [JK8], which are commented on in the section 2.3.

The second approach to prepare a nitrogen-rich film via magnetron sputtering, namely a sputtering of polyamide nylon, is described in [JK3]. While a clear presence of nitrogen in the films sputtered in Ar was detected, it was not as high as in the original polymer (8% in the films vs 12.5% in nylon (without hydrogen, not detectable by XPS)). This is a rather typical situation during the magnetron sputtering of polymers since some elements are more easily "lost" during the sputtering process. However, when N_2 was added into the process gas mixture, the nitrogen content increased (up to nearly 40%) in a similar way to [JK2].

One of the findings of this work was the detection of CO species being released from the sputtered polymer. This was found to be pretty common during all types of plasma sputtering/degradation/decomposition of polymer containing C=O groups. This knowledge was helpful later during the modelling of the process in [JK11], discussed in section 2.3.

A typical drawback of nitrogen-rich (and even more of amino-rich) coatings is their fast and intense aging when nitrogen in the film is gradually lost. Actually, after exposure of the films to ambient air (or even water, in the case of many potential bioapplications), a big part of this process is nearly instantaneous. The experimental setup used in [JK3] allowed comparison of XPS

elemental composition and infrared spectra of the films in-situ (as-deposited, without breaking vacuum) and after exposure to air (Fig. 2.5), and the above-mentioned fast changes were clearly detectable.

Later, a general understanding that increasing the concentration of $N(H_x)$– groups on the surface of the film above a few percent has little effect on increasing the effectivity of binding of the biomolecules – an original driver of the field. Also, other biomolecule-binding mechanisms have been developed for plasma polymers [19]. While the "race" to attain as high $N(H_x)$– groups content in the film as possible has basically ended in the context of biomedicine [20, 21], the techniques developed in the field remain useful [22].

2.2 Nanostructures

2.2.1 Nanocomposites

Nanocomposite thin films consist of a matrix material and a dispersed phase(s) (filler(s)), commonly in the form of nanoparticles (nanofibers, nanoplatelets etc.). There are numerous ways to synthesize such materials ([23, 24, 25]). In the case of organic-inorganic nanocomposites, the organic material (polymer, plasma polymer) typically serves as a matrix and inorganic material (metal, oxide) serves as a filler.

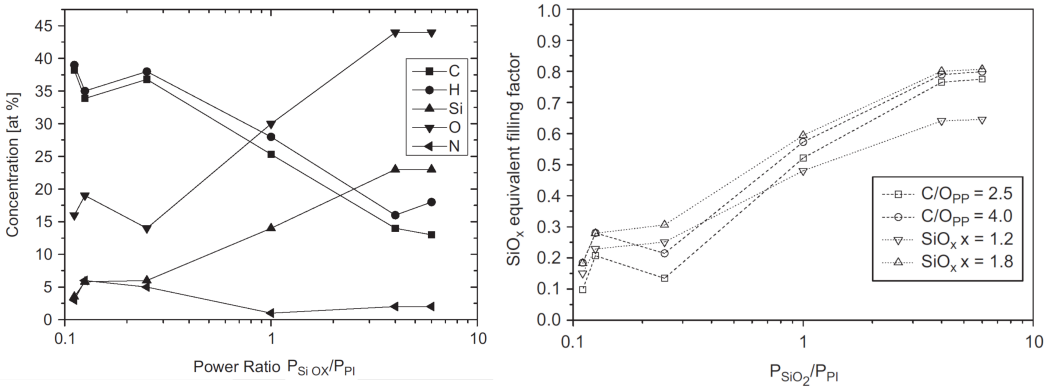

Figure 2.6: Properties of nanocomposite films prepared from dual magnetron sputtering of SiO_2 and polyimide in dependence on the magnetron power ratio. Left: RBS/ERDA elemental composition. Right: "Equivalent filling factor" established from RBS/ERDA data. Reproduced from [JK4].

The core parameter of any composite material is the volume fraction of each constituent (in the case of filler(s) so-called "filling factor"). In many cases, nanocomposites are prepared by techniques where the deposition of the matrix and deposition of the filler influence each other. This is a typical situation,

e.g. in the case of plasma polymerization combined with magnetron sputtering or sputtering the materials from two magnetrons. The cross-influence starts already at the magnetron sputtering since the diffusion of the other material can change the plasma properties at the other magnetron, influencing the deposition rate in this way. Moreover, due to mostly quite different surface energies of the film constituents combined with the possibility of atomic diffusion inside the material, the relation of the ratio of atomic fluxes to the volume fractions of constituents is often not straightforward. While the tunability of the nanocomposite properties is retained, the cross-influence of the deposition of matrix and filler does not allow a simple independent calibration of the deposition rates of constituents.

An example of solving this problem is presented in [JK4] in the case of simultaneous magnetron sputtering of polyimide and SiO_2. In the case where the direct (or semi-direct) measurement of volume fractions of film constituent is not available, but the full elemental composition of the film is measured, it is still possible to recalculate the elemental composition to the volume composition (Fig. 2.6).

2.2.2 Nanoparticles

First production of nanoparticles (size 1–10^2 nm) clearly identified as such was done over 150 years ago by Michael Faraday [26]. He used chemical means to prepare a colloidal solution of nanoparticles; a general approach performed and improved in many variants till today [27]. While there is a plethora of methods to prepare nanoparticles by "wet chemistry", there is also a rich field of nanoparticles prepared using physical methods, including vacuum-based techniques [28].

Production of nanoparticles is interesting in itself since nanoparticles (mostly due to their surface-to-volume ratio) have many interesting physical and chemical properties that often significantly differ from the properties of corresponding bulk material. In the chapter 2.2.1, the problem of limited control of self-assembly of nanocomposite from simultaneous atomic (or nearly atomic) fluxes of constituents was described. One of the possible solutions is to decouple the production of the matrix from the production of filler. Then, a separate source of nanoparticles is needed. Since there is a significant know-how on magnetron sputtering present at the author's department, a variant of magnetron-based gas aggregation cluster (nanoparticle) source ("GAS"/"Haberland source" [29]) was found most suitable (schematic image shown in Fig. 2.7). In this source, the

magnetron-sputtered material (section 2.1.3) forms nanoparticles in an aggregation chamber that are dragged by the flowing gas at $\sim 10^1$ Pa into the deposition chamber through a small orifice.

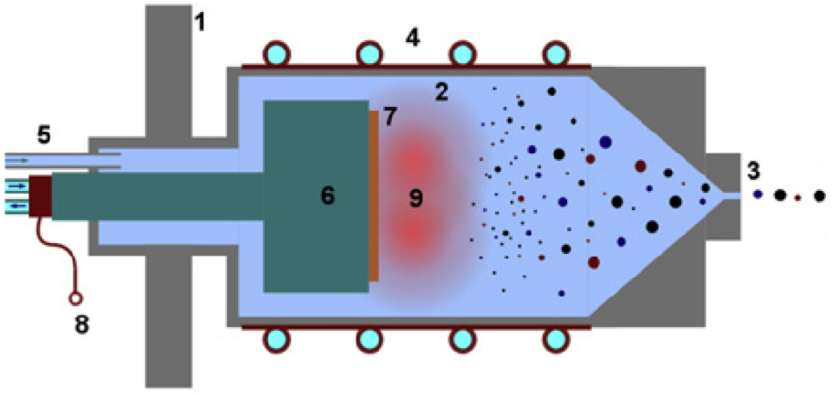

Figure 2.7: Scheme of the source of nanoparticles (GAS): 1–main chamber; 2–aggregation chamber; 3–orifice; 4–water cooling; 5–carrier gas inlet; 6–water-cooled magnetron; 7–target; 8–power source; 9–plasma. Reproduced/modified from [JK5].

In general, in gas aggregation sources, the main mechanism responsible for the nucleation and initial growth of nanoparticles (nanoclusters) is a "ternary" collision of an initial atom (or small cluster), "deposited" atom and a third atom (cooling gas, mostly inert (Ar, He)) that will carry away the heat of coalescence. Since true ternary collisions are rare, a more realistic nucleation scheme is a two-step process

$$A + A \rightarrow A_2^*$$

$$A_2^* + G_{cold} \rightarrow A_2 + G_{hot}$$

where A are the nucleating atoms and G is the cooling gas atom or molecule. Still, to overcome the (mostly thermal) processes that disassemble the particles, the nucleating atoms must be present in sufficient concentration to aggregate, forming an analogue of supersaturated vapours. The nucleation process can be more complex in the presence of reactive gases. In magnetron-based sources, nucleation on ions can be dominant [30]. A detailed description of the gas aggregation sources' physics and applications can be found e.g. in [31].

The original idea behind the magnetron-based gas aggregation nanoparticle sources was that the nanoparticles (charged by the magnetron plasma) would be electrostatically accelerated towards the substrate in order to "splash" fill the surface irregularities, decreasing this way the roughness and porosity of the growing thin film. Although working in principle, this

idea met a big obstacle to being employed commercially - the low deposition rate of the nanoparticles (originally ∼µg/h).

Several ways of improving the output of GAS were found, e.g. seeding the aggregation of nanoparticles with reactive gases [32, 33, 34] or even organic vapours [35]. Also, the original mass-filtering of nanoparticles can be dropped (and nanoparticle flux increased) in many practical applications, when broad size distribution o nanoparticles (FWHM value ∼ mean value) is not an issue. However, without a better understanding of processes inside GAS, the optimization of the nanoparticle production would still be hit-and-miss.

For a long time, most models of the growth of nanoparticles in GAS did not pay much attention to the details of the transport of nanoparticles inside the source itself via neutral gas. One of the problematic parts of GAS is the exit orifice. The gas flow inside the orifice is non-trivial by itself since there is a pressure drop of 2–3 orders of magnitude on a few mm (Fig. 2.8). The flow is quickly going from deeply subsonic to supersonic velocities and from continuous to free molecular regime, a challenging situation for theory and modelling. In this rapidly changing environment, the neutral gas drag accelerates nanoparticles, determining their velocity vector at exiting the source. Since this acceleration depends on the mass/cross-section ratio of the nanoparticles, a significant dependence of the velocity of the particles on their mass was predicted [36]. The velocity of nanoparticles is also important for their sticking coefficient and adhesion to the substrate and the morphology of the film grown from them.

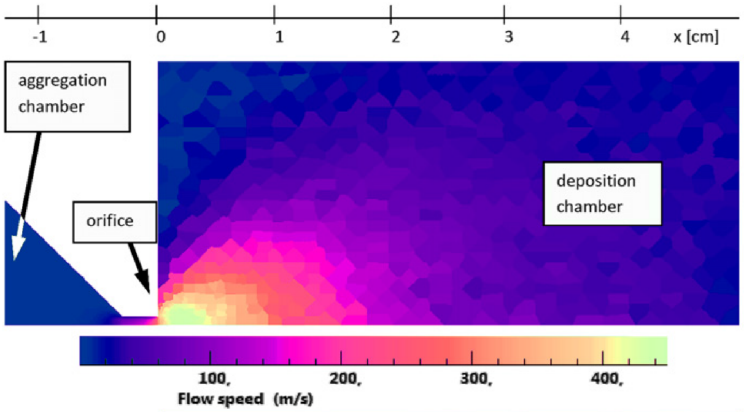

Figure 2.8: 2D map of the gas velocity near the GAS orifice of the nanoparticle source obtained using Direct-Simulation-Monte-Carlo (DSMC) modelling. The bottom line of the map is the axis of symmetry. Reproduced from [JK5].

A very simple electrostatic deflection setup (Fig. 2.9) coupled with post-deposition analysis of the sizes of the deflected particles was used to determine the velocity of Ag nanoparticles within three orders of magnitude in

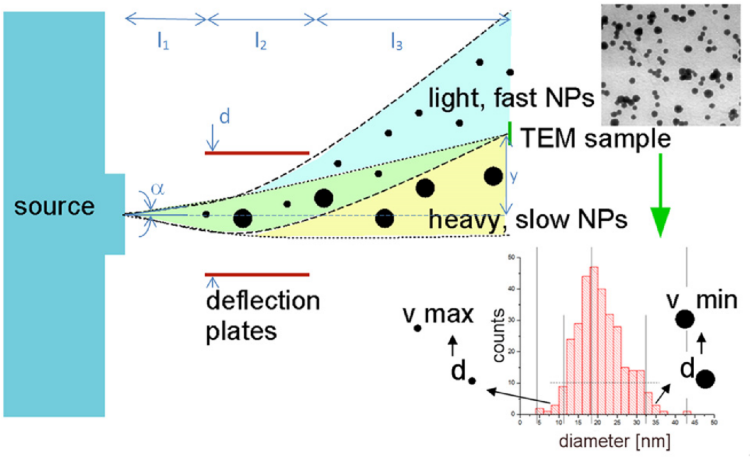

Figure 2.9: General layout of the electrostatic deflection setup used to measure the velocities of the nanoparticles exiting GAS. For a given deflection voltage and a given sample location, the lightest and heaviest particles obtained from the size distribution histogram are used to estimate the maximal and minimal values of the velocity of the particles of the corresponding size, respectively. Reproduced from [JK5].

mass [JK5]. The simple geometry of the setup can be treated analytically. The deflection distance y of the particle can be expressed as

$$y = (l_1 + l_2 + l_3)sin\alpha - \frac{Uq}{dmv_0^2}\left(\frac{l_2^2}{2} + l_2 l_3\right)$$

where l_1, l_2, l_3, d describe the geometry of the experiment (Fig. 2.9), α is the initial angle of flight of the particle, U is the deflection voltage between the plates, q is the charge of the particle, m is the mass of the particle and v_0 is the velocity of the particle. This expression would be sufficient to obtain the expected dependencies of y on other parameters, but an integration of the motion of particles using a numerical model of the electric field was used to deal with the edge effects of the finite length of the deflection plates.

Since there was necessary to operate with several initial assumptions about the process, an independent "hybrid" model of nanoparticle motion allowing a partial cross-checking of the interpretation of the experimental data was developed. It was based on analytical expressions for gas atom-nanoparticle impulse transfer integrated on the background of numerical solution of the gas flow (Fig. 2.8).

The dependence of the velocity of the nanoparticles on their mass was found to be quite significant (Fig. 2.10). While all the measured velocities were compatible with the expected "soft landing" regime of nanoparticles on the substrate, the velocity ratio between fastest and slowest nanoparticles was 10:1.

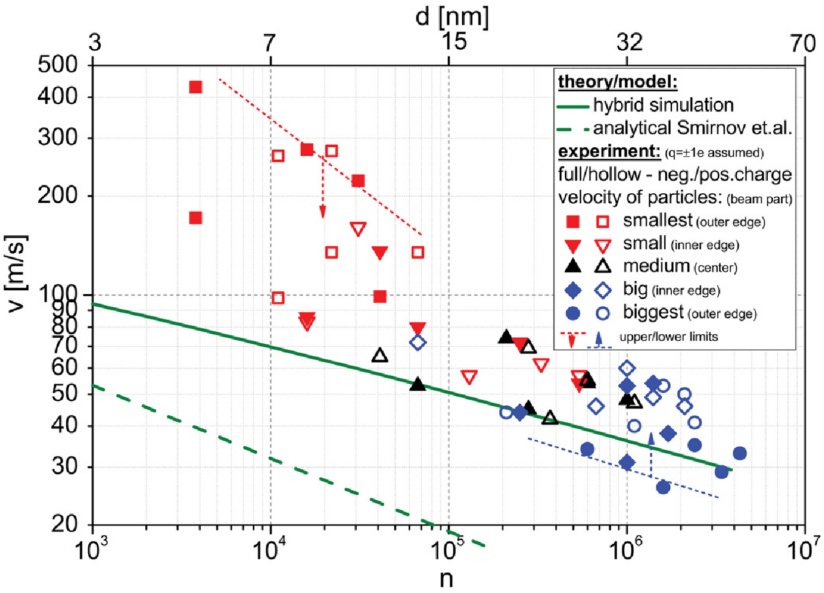

Figure 2.10: Modelled and experimentally determined values of the velocity of the nanoparticles exiting GAS. Velocities vs the number of atoms in the particle (or the diameter of the particle) are shown. Reproduced from [JK5].

Velocities of the nanoparticles were subsequently measured in a narrower range of masses using mass spectrometry [37] and more recently characterized using a slotted disc filter [38]. Understanding the influence of the gas flow on the nanoparticles was important e.g. for the preparing of core–shell nanoparticles [39]. There, the pressure-tuned deceleration of nanoparticles allowed for optimizing of the in-flight shell deposition.

The influence of gas flow was found to be important also inside the GAS itself. The motion of very small (few nm) nanoparticles was demonstrated to be dominated by the Brownian motion [40], and the overall performance of GAS also depends on the internal configuration of the walls, orifice and gas inlet [41, 42, 43].

The above-mentioned deflection–velocity experiment [JK5] also gave additional insight into the question of the charge on the nanoparticles. The velocity of the nanoparticles was not dependent on the polarity of their charge, confirming that at least near and out of the GAS orifice the neutral gas drag is the driving force on the nanoparticles. Through additional reasoning, an interesting hint on the charge of nanoparticles exiting GAS was obtained. Most (or nearly all) charged nanoparticles must be charged only by plus/minus one elementary charge. While this was suspected (and to some extent experimentally confirmed) before, the broad range of masses of nanoparticles covered in this experiment confirmed this to be likely a general rule in magnetron-based GAS. The zero or only single elementary charge of nanoparticles exiting GAS

is not a trivial statement since the low-temperature plasma easily charges any adjacent surfaces (section 2.1.2), including nanoparticles.

In the simplest treatment, when the particle of radius r is considered to be a spherical capacitor, its equilibrium charge is

$$q_r = 4\pi\epsilon_0 r V_r$$

where V_r is a floating potential given by the balance of electron and ion flux. The floating potential for typical low-pressure plasmas in argon is approximately $V_r \sim 5T_e$, where T_e is the electron temperature in eV. Thus in the active plasma with $T_e \sim 1\,\mathrm{eV}$ one shall expect a charge of about $1e$ per 1 nm of the diameter of the particle, in a seemingly clear contradiction with the single charge of the nanoparticles found in [JK5].

The reason for this discrepancy is simple - the active plasma zone in magnetron-based GAS represents only a small fraction of the volume of the aggregation chamber. The rest of its volume fills mostly a weak afterglow (or auxiliary, [36]) plasma. Then the equilibrium charge of the nanoparticles drops quickly towards zero with nearly symmetrical fluctuations to plus/minus single elementary charge [44].

However, to have a clear picture of the plasma–nanoparticle interaction, good experimental data on the plasma parameters inside GAS are needed. One of the mostly neglected problems in the physics of magnetron-based GAS is the unavoidable coupling of the nanoparticle nucleation&growth and electrostatic forces-driven transport, especially in the initial stages of the process of nanoparticle formation.

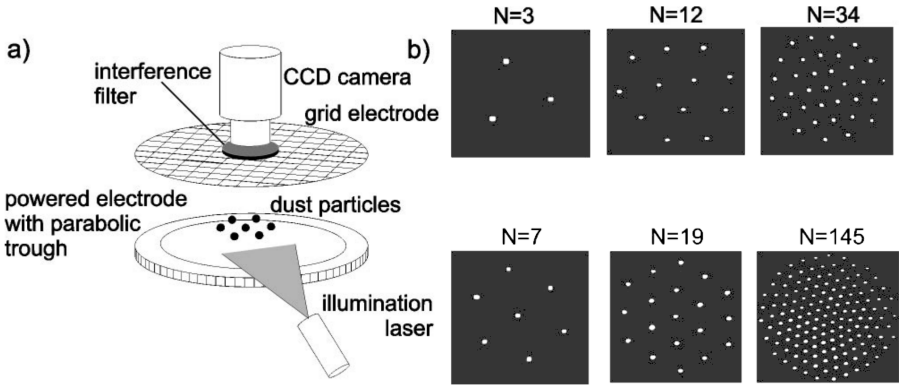

Figure 2.11: Self-assembled Coulomb "plasma crystal" of microparticles charged by (and levitating in) the low-pressure plasma. Reproduced from [45].

The importance of this growth-charging-transport coupling is quite well known from the field of so-called "dusty/complex plasmas" (monography review can be found e.g. in [46]). A large amount of data and models was

accumulated mostly on the micrometers-sized particles in a normal glow discharge. The effect of trapping of charged particles was studied and utilized e.g. to make so-called "plasma crystals" (Fig. 2.11) or even employed to characterize the local plasma parameters [47].

Going down several orders of magnitude in particle size, quantitative characterizations of plasma–nanoparticles interaction become more scarce. Most such works were done on particles grown via plasma polymerization (section 2.3) from gaseous precursors where the source of material (typically hydrocarbon molecules) is decoupled from the source of the plasma [48, 49]. In such experiments, nanoparticles significantly influence on the plasma since the they very effectively scavenge the electrons.

The situation is even more complicated in the case of nanoparticles grown in the magnetron discharge from the sputtered material. Conditions in the plasma near the erosion track of the magnetron govern the sputtering rate of the material needed for nucleation and growth of nanoparticles. The plasma parameters vary significantly within this region, which is not an easy target for direct measurement of plasma parameters even in the normal particle-free case.

Another important issue is that the magnetron discharge in GAS is typically operated at higher pressures (10^1–10^2 Pa) than it is common for most sputtering processes (10^{-1}–1 Pa), and thus even the basic data on plasma parameters of magnetron discharge at GAS conditions were rather minimal [50]. There was a clear motivation to obtain such data and – if possible – to quantify the role of the nanoparticles.

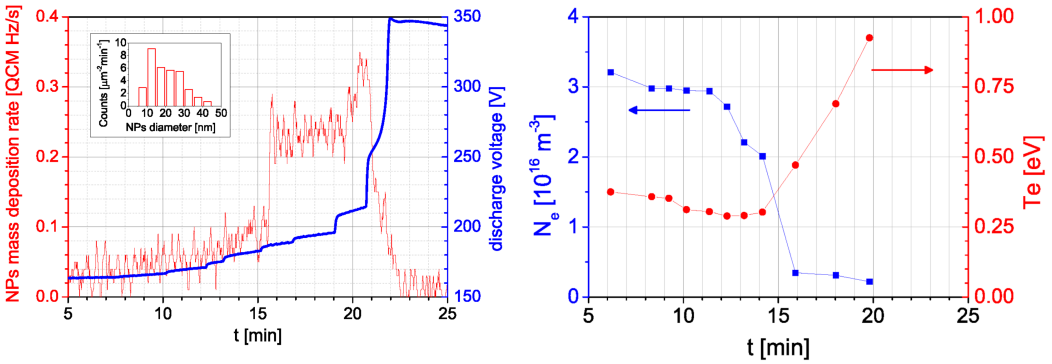

Figure 2.12: Influence of the presence of nanoparticles triggered by the oxygen admixture on the magnetron discharge shown as time dependencies of measured quantities during one continuous experiment. Left: Magnetron voltage and deposition rate of nanoparticles (typical size distribution shown in the inset). Right: Plasma density and effective electron temperature 30 mm from the magnetron plane. Reproduced from [JK6].

As mentioned previously, adding a small amount of reactive gases, like oxygen, into GAS can sometimes trigger increased nanoparticle production. In the case of nanoparticles from (sub)oxides of reactive metals like aluminium or titanium, it can lead to a rather abrupt "switch on" of the nanoparticle formation with minimal changes in other process parameters [34, 51]. While this sensitivity can also complicate keeping the operation of the GAS stable, it offers an opportunity to characterize the accompanying change in the plasma parameters. In this case, we can assume that the detected changes are mostly caused by the presence of nanoparticles and their interactions with the plasma.

As the model process, the production of Ti/TiO_x nanoparticles from reactive Ti sputtering in Ar with a few % O_2 admixture was chosen [JK6]. When the Ti target was in the metallic state, no production of nanoparticles was observed. With increasing O_2 admixture, at the onset of oxidation of the target, nanoparticles appeared. Their production increased until the target became quickly fully oxidized (known effect from reactive sputtering [52]), and there was not enough material sputtered to form nanoparticles anymore.

Although direct measurement of plasma parameters using a Langmuir probe [53] was challenging in the highly depositing plasma, the influence of nanoparticles on the plasma was clearly detected (Fig. 2.12). The plasma density dropped by an order of magnitude, and electron temperature increased threefold.

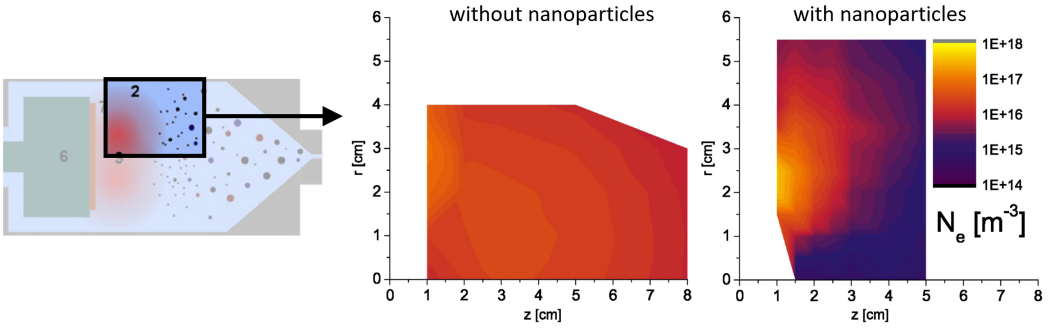

Figure 2.13: 2D maps of electron density and electron temperature inside the GAS. Left: Schematic representation of the mapped area in GAS. Middle: Plasma density without nanoparticles. Right: Plasma density with nanoparticles. The erosion zone of the magnetron is at x=0 cm and r=2 cm. Reproduced and adapted from [JK5] and [JK6].

With the experience gained, it was possible to operate the Langmuir probe long and reliably enough to fully utilize the GAS with a movable magnetron to prepare a 2D maps of the plasma parameters (Fig. 2.13; for the maps of all parameters, see [JK6]). The influence of the presence of nanoparticles on the plasma was even more clear, since the effect could be localized. Observed

changes above the erosion zone were expected since most of the material to form nanoparticles comes through this area. However, even more pronounced changes were found just above the center of the magnetron target. The electron density depletion and the rise in the electron temperature were most pronounced there, suggesting a high concentration of nanoparticles in a supposedly "empty" region. Interestingly, even the map of the plasma potential suggests that the negatively charged particles would be expelled from the plasma ring both along the axis of the magnetron (as expected) and towards the axis and the centre of the target.

To the author's knowledge, the work [JK6] provided the first 2D map dataset of plasma parameters in GAS, including the direct quantification of the influence of the presence of nanoparticles. Good data of a similar kind still remain scarce [54].

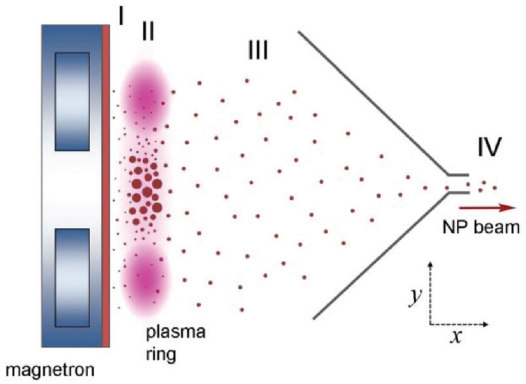

Figure 2.14: Different zones of the growth of nanoparticles in GAS identified by the in-operando SAXS: I–nucleation and growth, II–trapping in the capture zone, III–transport of small nanoparticles along the GAS, IV–transport of small nanoparticles outside the GAS. Reproduced from [JK7].

The detection of the changes above the centre of the magnetron was not coincidental. The authors' group performed a series of experimental campaigns at Deutsches Elektronen-Synchrotron DESY (Hamburg, Germany), and the author is proud to have one of the key roles in the design, performing and interpretation of those experiments. The measurements utilized Small-Angle X-ray Scattering (SAXS) in order to detect the growth of nanoparticles in GAS in-operando, in-situ. Previously, an X-ray characterization was done on nanoparticles outside the source [55]. While this was an outstanding feat, measurements inside the GAS were challenging in a different way due to the background scattering on the gas, X-ray windows contamination, synchronization of the setup etc.

When the technical obstacles were solved, an important finding appeared – a large amount of nanoparticles was found to be trapped in the front of the

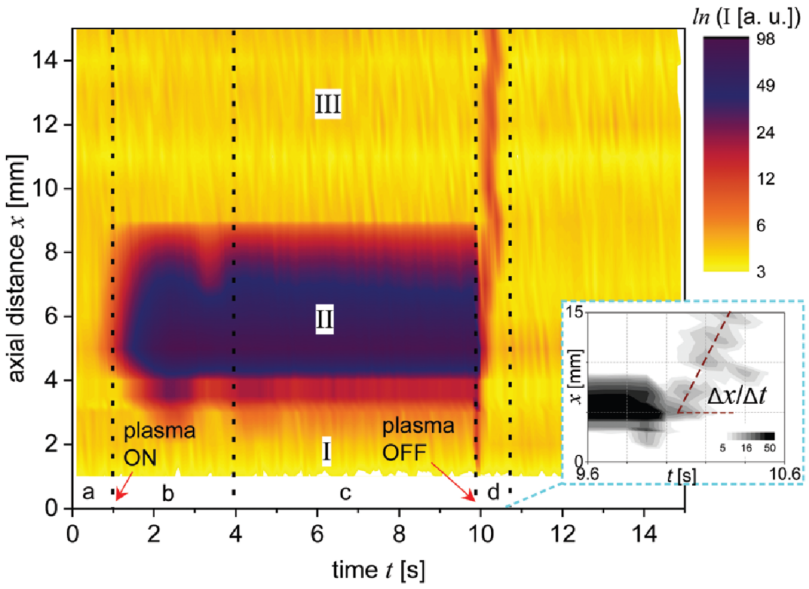

Figure 2.15: Time-resolved X-ray scattering intensity in GAS. Growth and trapping of nanoparticles above the magnetron (zone II; x=4–8 mm) and detected release and transport of nanoparticles after the discharge is switched off shown (enhanced view presented in the inset). Reproduced from [JK7].

centre of the magnetron [JK7]. These trapped particles were several times bigger than the "common" nanoparticles (∼80 nm vs ∼20 nm), holding a big share of the volume of the sputtered material. The general "map" of the inside of the magnetron-based GAS had to be revised (Fig. 2.14). Additional time-resolved data have shown that the formation of the trapped cloud takes ∼1 s, and the release of the particles after the discharge was switched off was clearly observed (Fig. 2.15). Later measurements have studied the dynamics of the growth of nanoparticles in this trapped cloud and helped to explain some periodic instabilities sometimes observed during GAS operation that were previously mostly overlooked [56]. Soon after the SAXS measurements, the trapping of nanoparticles in GAS was also confirmed using UV-VIS spectrophotometry via plasmon absorption on Ag nanoparticles [57].

These findings helped to explain some limitations of the output of magnetron-based GAS. This trapping effect was found to happen especially during conditions when the production rate of nanoparticles increases (especially with increasing pressure in the aggregation chamber), and the trapping is one of the key limiting factors to increase it further.

While the general mechanism of the trapping is understood as a direct analogy of the effects known from the field of complex plasmas, the full quantitative modelling remains challenging. Nevertheless, knowledge about the existence of this effect has already helped to increase the performance

of magnetron-based GAS. Tailored mitigation of the trapping through optimization of the gas flow to manipulate or disrupt the cloud of trapped nanoparticles was already demonstrated [58, 59]. Significant improvement in the deposition rate was shown. Improvement of GAS performance will also be helpful in producing of nanocomposites (section 2.2.1) with a high deposition rate of the plasma polymer matrix (section 2.3).

2.3 Plasma polymers

Plasma polymers are materials prepared from organic molecules using non-equilibrium plasma chemistry. They are typically prepared as thin films. While their formation was noticed decades earlier, their usefulness was recognized in the 1950s and 1960s [60, 61].

The plasma polymerization[1] process typically starts with introducing a monomer in a gaseous state into low-temperature plasma where it is ”activated”. The ”activation” typically means fragmenting the monomer molecules by collisions with high-energy plasma species, forming mostly reactive radicals. Through their reactions, longer macromolecules are formed either already in the volume of the plasma (to form nanoparticles (section 2.2.2)) or (more typically) on the substrate. The resulting material is then significantly different from the original monomer, and the molecular structure of the film can even be considered to be partially disordered (Fig. 2.16). On the other hand, the process is inherently solvent-free and crosslinking in the macromolecular structure is very easy.

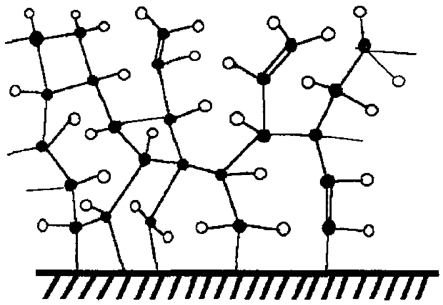

Figure 2.16: Example of the possible structure of plasma polymer prepared by magnetron sputtering of polytetrafluoroethylene based on its polarized infrared spectra. Reproduced from [13].

In contrast, classical chemistry (”wet” chemistry) methods can prepare materials with regular, even complex molecular structures. Unfortunately, sol-

[1]Note: The term ”plasma polymerization” broadly overlaps with the term ”plasma-enhanced chemical vapour deposition - PECVD”. The author prefers the former term.

vents or crosslinking agents used during polymer synthesis can form residues in the material, and a high degree of crosslinking is often quite tricky to obtain.

One of the main limiting factors in the preparation of plasma polymer with complex molecular structures is the limit of the molar mass of the monomer that needs to be introduced into plasma in a gaseous state. Monomers with more complex structure typically have too low vapour pressure to be practical, so generally simple low-molar mass monomers (10^1–10^2 g mol^{-1}) must be used (note: rather extreme case of this issue is the magnetron sputtering of polymers, as described in the section 2.1.3).

One of the ways how to overcome this limitation of plasma polymerization is to use a classical polymers as a source of comparatively high molar mass oligomers produced "in-situ".

The first use of such an approach for depositing thin films at low pressures was probably demonstrated on polypropylene and polytetrafluorethylene in the 1960s [62, 63]. In that case, the polymer material was put in a heating cell and heated to the point of the onset of thermal degradation. The polymer chains experience thermal scission, releasing a stream of oligomer vapours that form a soft thin film on the substrate. Such films were proposed to serve as dielectric barriers [64].

Later, the ionized cluster beam deposition technique was adapted to accommodate an evaporator with a polymeric material [65, 66]. Compared to films from pure evaporation, the films exhibited an improved mechanical properties, but the details of their molecular structure remained hazy.

Another way to release heavy precursors into plasma is to sublimate it through the thermal effects of the glow discharge plasma [67, 68], utilizing one of the effects of plasma treatment (section 2.1.2). More recently, remote plasma-assisted vacuum deposition (combining evaporation of complex molecules and an afterglow plasma) was developed [69, 70].

In the case of magnetron sputtering, a high temperature of the surface of the target is usually to be avoided. In the case of sputtering of polymers, due to their limited thermal conductivity, the local temperature on the target can rise quite easily. During the sputtering of polyethyelene target at high power, a hint of local "co-evaporation" of material from the erosion zone was found [71].

This effect was studied in more detail during the sputtering of low-density polyethylene and polyisobutylene [JK8]. These materials were chosen intentionally for to their lower melting temperatures. Indeed, the "co-evaporation" regime was observed for both materials. The infrared spectra obtained from the films prepared at this deposition regime were nearly the same as for the

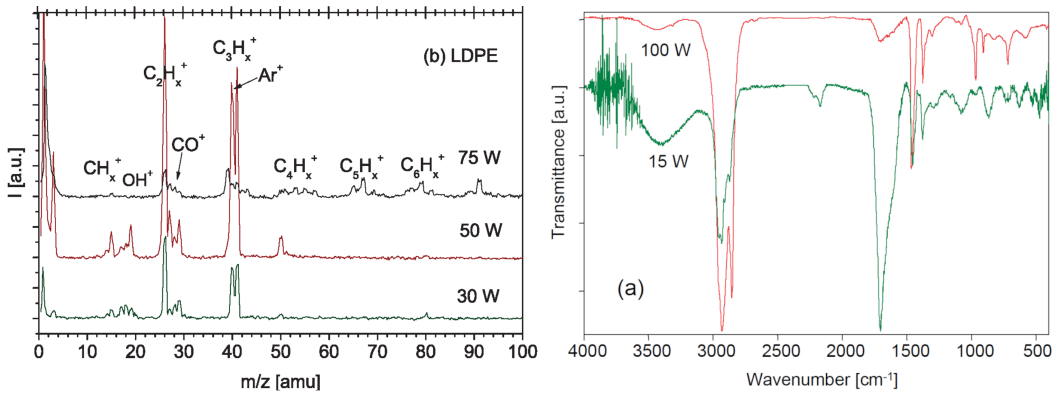

Figure 2.17: Magnetron sputtering of low-density polyethylene target with co-evaporation at power $\geq$ 75W. Left: Mass spectra of the process gas. Right: Infrared spectra of plasma polymer thin films. Reproduced from [JK8].

original polymer (Fig. 2.17). The mass spectra of the gas have shown a significantly increased amount of heavier C_xH_y fragments (M_r>50 g mol^{-1}). While the thin films prepared by this technique were found interesting, the inherent instability of the process and very short target lifetime made systematic study challenging. There is no direct control over the local surface temperature of the target in this "thermal runaway" regime.

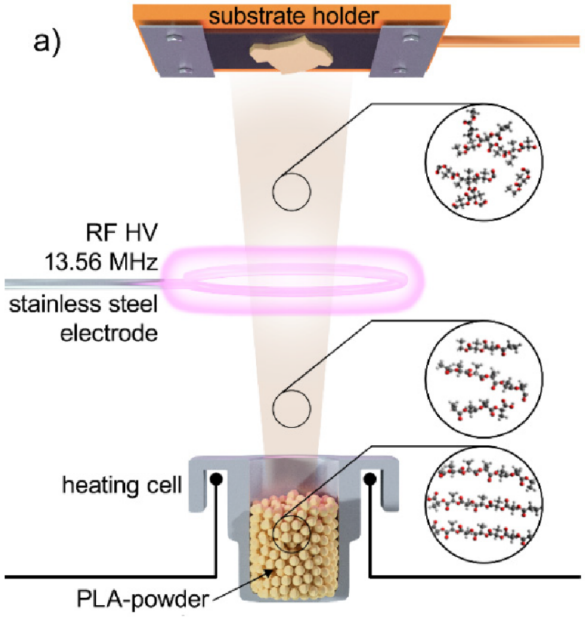

Figure 2.18: Experimental set-up used for Plasma-Assisted Vapour Thermal Deposition (PAVTD) (demonstrated using polylactic acid). Reproduced from [JK11].

To study the plasma polymers prepared from these "long" hydrocarbon fragments, the idea of thermal degradation of the polymer in a dedicated crucible was revived and combined with the utilization of an auxiliary plasma

source to induce plasma polymerization [72]. A more recent version of a similar experimental configuration is shown in Fig. 2.18.[2]

In the subsequent works, it was found that the oligomers released from the thermal degradation of the polymeric material ("precursor") have indeed significantly heavier molar masses than the common compounds used in plasma polymerization from the gas phase (10^2 g mol^{-1}–10^3 g mol^{-1}). The thin films prepared using PAVTD can then retain most of the molecular structure of the classical polymers and tune it in a broad range by changing the power in (re)polymerizing plasma. This feature was utilized e.g. for preparation of non-fouling (protein non-adsorbing) films [73] or as a tool to study the self-organization of domains of dissimilar polymers [74]. The possibility of retaining a big share of "classical" polymer chemistry and polymer physics was demonstrated.

The author of this thesis perceived the potential of PAVTD and he was able to obtain two research grants to explore this technique in more detail. Two key drivers were the study of the limits of tunability of the properties of the films and the possibility of gaining new insights into the process of plasma polymerization in general.

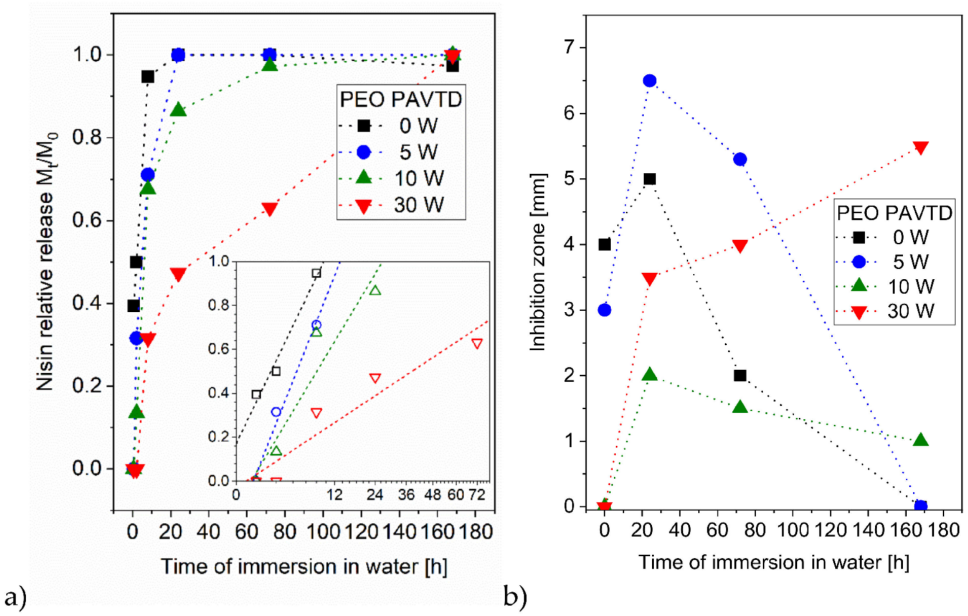

a) b)

Figure 2.19: Time dependence of release of bacteriocin nisin from the drug-loaded PVA film with tunable PEO PAVTD films overcoat. a) Relative release of nisin into water (power law fits in the inset) b) Antimicrobial activity against Staphylococcus aureus (qualitatively: wider inhibition zone = higher antimicrobial effect). Reproduced from [JK9].

[2]This deposition principle can be found under various names, the author of this thesis prefers to use the term Plasma-Assisted Vapour Thermal Deposition (PAVTD).

The transition region between the films consisting of oligomers and fully crosslinked plasma polymers seemed promising for potential biomedicinal applications of the films. At the author's department, there was already a know-how on using PAVTD with polyethylene oxide (PEO) as a precursor. A finding obtained on this material was that the molar mass of the original polymer plays only a minor role in the properties of the resulting films. The major influence was the plasma power used [JK9].

One of the basic problems in drug delivery systems, including coatings, is regulating the release rate of the drug [75]. The PEO-like PAVTD films were utilized as an overcoat layer over a drug-loaded film (soluble polyvinyl alcohol loaded with nisin, a small protein with a bactericidal effect). Control of the release rate of nisin in water was demonstrated on the nisin release dynamics as well as on the bactericidal effect of the films (Fig. 2.19). The latter test is important in showing that the released protein drug does not lose its tertiary structure during storage or release.

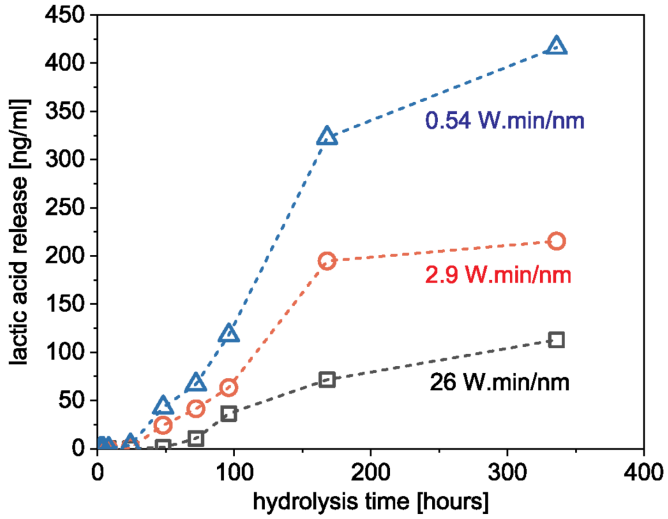

Figure 2.20: Tunable hydrolysis rate of PLA-like PAVTD films prepared at varying effective plasma power. Reproduced from [JK10].

Most of the recent work was then focused on polylactic acid (PLA). The work [JK10] demonstrated that PAVTD could be effectively described using a variant of so-called Yasuda parameter Y for gas-phase plasma polymerization [76, 77].

$$Y = \frac{W}{FM}$$

where W is the plasma power in the polymerization zone, F is the monomer molar flow and M is the molar mass of the monomer. Y represents the most simple scaling parameter in plasma polymerization, basically denoting energy expended on the unit mass of the material.

The original Yasuda parameter counts on volatile precursors that do not form a film, unless they are activated (converted into radicals) in a plasma. In PAVTD, the situation is different. Even without the plasma, the heavy oligomers condense (and partially spontaneously polymerize) readily on any surface. The flow of the monomer can then be directly correlated with the film deposition rate, so in the work [JK10], it was demonstrated that a parameter "effective plasma power" P_{eff}

$$P_{eff} = \frac{W}{dh/dt}$$

where W is the plasma power and dh/dt is the deposition rate (in thickness per time). It was demonstrated that even a diverse set of experiments (caused by higher sensitivity of PLA to thermal fluctuation in the crucible compared to PEO) could be then clearly sorted and dependencies of composition and stability on P_{eff} can be demonstrated (Fig. 2.20, note that detection of released lactic acid means that at least some part of the original polymer chains must have been retained).

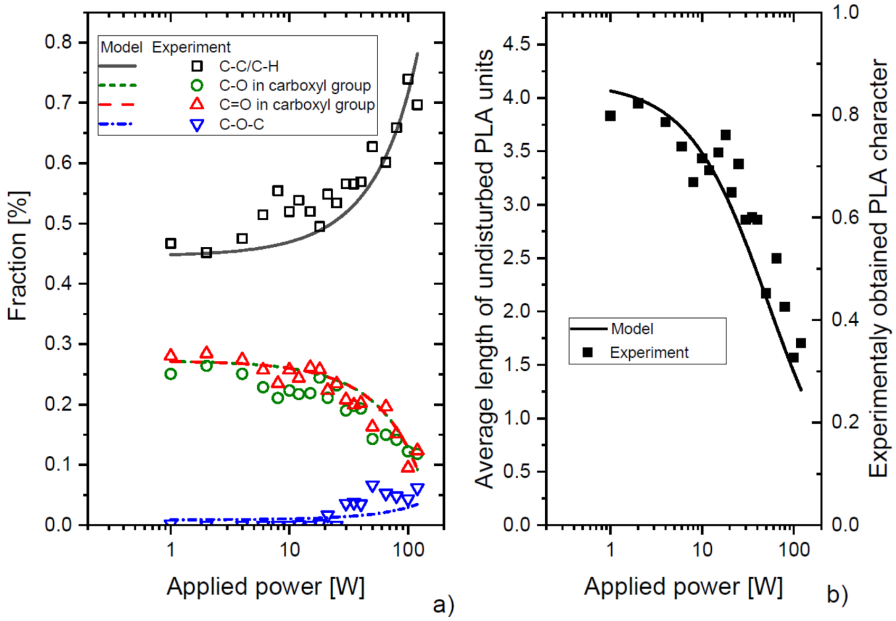

Figure 2.21: Comparison of a model of the composition of PAVTD-prepared PLA-like plasma polymer with experimental data for varying discharge power. a) fractions of various types of subunits b) average length of "undisturbed" parts of PLA chain. Reproduced from [JK11].

With gradually improved stability of the setup, more precise experiments with PLA-like PAVTD films were possible on a larger set of samples [JK11, JK12], allowing utilization of "volume" diagnostics methods like gel permeation chromatography (GPC) or nuclear magnetic resonance (NMR), that are

not usually possible to be employed on plasma polymers. Using the combined data from XPS and NMR, it was possible to get a surprisingly clear picture of the molecular structure of the films (Fig. 2.21). This structure could be well approximated by the original PLA chain interleaved with ether-like and hydrocarbon-like units in the chain. With increasing plasma power, the amount of "modified" units increased, and the average length of the original PLA chains decreased. At the lowest plasma powers, the length of undisturbed parts of PLA chain shall represent the length of the thermally released oligomers from the crucible. A very good agreement between values obtained from XPS+NMR and GPC was then found.

Moreover, elucidation of the molecular structure allowed the development of the numerical model of this specific plasma polymerization process. Utilizing knowledge gained on other oxygen-containing polymers (section 2.1.3), the model could reproduce the dependency of the film composition on the plasma (re)polymerization power surprisingly well. Such predictive models are not common in the field of plasma polymerization and they are mostly more complicated [78, 79, 80].

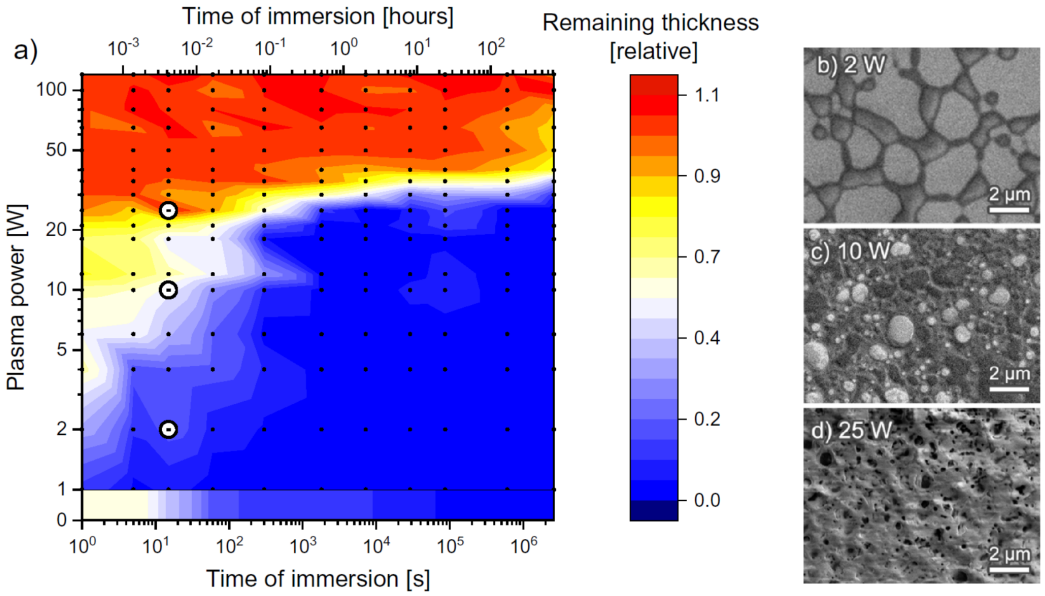

Figure 2.22: Tunable stability of PLA-like PAVTD films prepared at varying discharge power. a) Stability in water for varying times of immersion indicated by relative remaining thickness (gel volume fraction) b–d) SEM images obtained after 15-second immersion in water and drying. Reproduced from [JK12].

The same PLA-like films were also characterized by thermal stability and especially by the stability in water. A huge – over 5 orders of magnitude – range of tunability of the characteristic time for the stability in water was

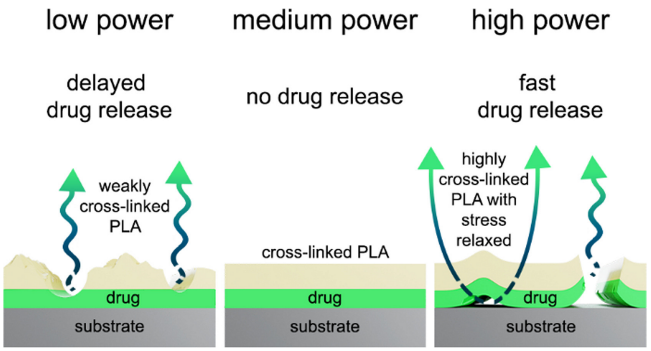

Figure 2.23: Schematic representation of two distinct mechanisms leading to the release of the drug from the carrying layer overcoated by PLA-like PAVTD films prepared at various discharge powers. Reproduced from the graphical abstract of [JK12].

achieved, from sub-seconds to weeks (Fig. 2.22). At low polymerization plasma power, the oligomer wash-out is the dominant process. After attaining of the gelation point, when the free chains start to disappear, the stability clearly increases. The SEM images show that the film is not fully homogeneous and forms more and less stable domains.

Interestingly, the films prepared without plasma are more stable than the films prepared at very low plasma power. There seems to be competition between the oligomers' fragmentation and their polymerization. This top-down vs bottom-up competition is a part of the ongoing studies.

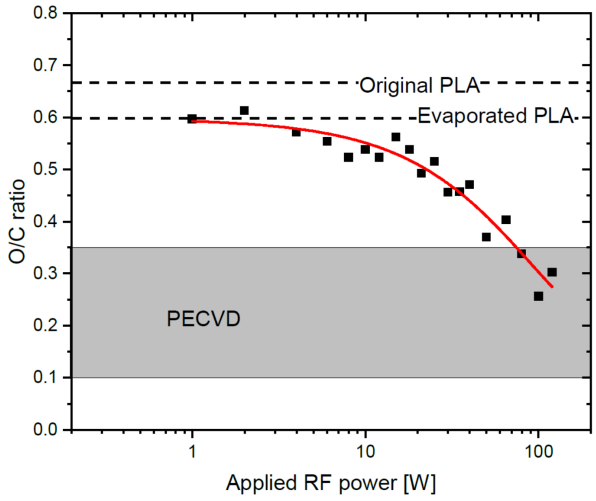

Figure 2.24: Comparison of oxygen/carbon content ratio of classical PLA polymer, common PLA-like plasma polymers (PECVD) and PAVTD films [81, 82]. Reproduced from [JK11].

The broad tunability of the PLA-like films were also tested as the drug release-delaying films. In a similar fashion like in [JK9], nisin-loaded PVA film was overcoated by PLA-like layer and then the release kinetics of nisin into the

water was measured. The situation was more complex than in the case of PEO-like films. Two different drug release mechanisms were identified (Fig. 2.23). Still, the tunability of the release times from minutes to hours was shown.

These experiments have clearly shown that PAVTD is a very useful tool to produce and study materials that are not easily obtainable either via classical chemistry or common plasma polymerization (Fig. 2.24). In a way, it can be said that PAVTD bridges the gap between classical and plasma chemistry .

3. Concluding remarks and outlook

Low-temperature plasma physics, including plasma chemistry, is a very diverse field. In this thesis, its author tried to cover several more or less closely related problems that can lead – or already have led – to better understanding of the processes in the plasma, on the plasma-adjacent surfaces and the processes connecting these domains. The classical low-temperature plasma physics in atomic or simple molecular gases is not a simple field in itself. The incorporation of nanostructures and macromolecules into the plasma processes makes the related physics only more diverse and fascinating.

Th author's personal mid-term plan is the to improve the PAVTD technique even further, to utilize it as a study tool both on the borders of plasma polymerization and the borders of classical polymer physics. Moreover, in terms of material science, by combining PAVTD with the advanced vacuum-based methods of producing nanoparticles, new types of nanocomposite structures can be possible.

4. Selected publications

[JK1] J. Kousal, A. Shelemin, O. Kylian, D. Slavínská, and H. Biederman. In-situ monitoring of etching of bovine serum albumin using low-temperature atmospheric plasma jet. *Applied Surface Science*, 392:1049–1054, 2017. DOI: 10.1016/j.apsusc.2016.09.135.

[JK2] J. Hanus, J. Kousal, A. Choukourov, H. Biederman, and D. Slavinska. RF Magnetron Sputtering of Poly(propylene) in a Mixture of Argon and Nitrogen. *Plasma Processes and Polymers*, 4:S806–S811, 2007. DOI: 10.1002/ppap.200731910.

[JK3] J. Kousal, J. Hanus, A. Choukourov, O. Polonskyi, H. Biederman, and D. Slavínská. In Situ Diagnostics of RF Magnetron Sputtering of Nylon. *Plasma Processes and Polymers*, 6:S803–S807, 2009. DOI: 10.1002/ppap.200932001.

[JK4] M. Drábik, J. Kousal, Y. Pihosh, A. Choukourov, H. Biederman, D. Slavínská, A. Macková, A. Boldyreva, and J. Pešička. Composite SiO_x/hydrocarbon plasma polymer films prepared by RF magnetron sputtering of SiO_2 and polyimide. *Vacuum*, 81(7):920–927, 2007. DOI: 10.1016/j.vacuum.2006.10.013.

[JK5] J. Kousal, O. Polonskyi, O. Kylian, A. Choukourov, A. Artemenko, J. Pešička, D. Slavínská, and H. Biederman. Characterization of nanoparticle flow produced by gas aggregation source. *Vacuum*, 96:32–38, 2013. DOI: 10.1016/j.vacuum.2013.02.015.

[JK6] J. Kousal, A. Kolpaková, A. Shelemin, P. Kudrna, M. Tichý, O. Kylián, J. Hanuš, A. Choukourov, and H. Biederman. Monitoring of conditions inside gas aggregation cluster source during production of Ti/TiO_x nanoparticles. *Plasma Sources Science and Technology*, 26(10):105003, 2017. DOI: 10.1088/1361-6595/aa88e8.

[JK7] J. Kousal, A. Shelemin, M. Schwartzkopf, O. Polonskyi, J. Hanus, P. Solař, M. Vaidulych, D. Nikitin, P. Pleskunov, Z. Krtouš, T. Strunskus, F. Faupel, S. V. Roth, H. Biederman, and A. Choukourov. Magnetron-sputtered copper nanoparticles: lost in gas aggregation and found by in situ X-ray scattering. *Nanoscale*, 10(38):18275–18281, 2018. DOI: 10.1039/C8NR06155F.

[JK8] J. Kousal, J. Hanuš, A. Choukourov, P. Hlidek, H. Biederman, D. Slavínská, and J. Zemek. RF magnetron sputtering and evaporation of polyisobutylene and low density polyethylene.

Surface & Coatings Technology, 200(1–4):472–475, 2005. DOI: 10.1016/j.surfcoat.2005.02.107.

[JK9] J. Kousal, J. Sedlaříková, Z. Kolářová-Rašková, Z. Krtouš, L. Kučerová, A. Hurajová, M. Vaidulych, J. Hanuš, and M. Lehocký. Degradable Poly(ethylene oxide)-Like Plasma Polymer Films Used for the Controlled Release of Nisin. *Polymers*, 12(6):1263, 2020. DOI: 10.3390/polym12061263.

[JK10] J. Kousal, Z. Krtouš, Z. Kolářová-Rašková, J. Sedlaříková, J. Schaefer, L. Kučerová, A. Shelemin, P. Solař, A. Hurajová, H. Biederman, and M. Lehocký. Degradable plasma polymer films with tailored hydrolysis behavior. *Vacuum*, 173:109062, 2020. DOI: 10.1016/j.vacuum.2019.109062.

[JK11] Z. Krtouš, L. Hanyková, I. Krakovský, D. Nikitin, P. Pleskunov, O. Kylián, J. Sedlaříková, and J. Kousal. Structure of Plasma (re)Polymerized Polylactic Acid Films Fabricated by Plasma-Assisted Vapour Thermal Deposition. *Materials*, 14(2):459, 2021. DOI: 10.3390/ma14020459.

[JK12] Z. Krtouš, J. Kousal, J. Sedlaříková, Z. Kolářová-Rašková, L. Kučerová, I. Krakovský, J. Kučera, S. Ali-Ogly, P. Pleskunov, and A. Choukourov. Thin films of cross-linked polylactic acid as tailored platforms for controlled drug release. *Surface & Coatings Technology*, 421:127402, 2021. DOI: 10.1016/j.surfcoat.2021.127402.

4.1 Author's role(s) and key activities/contributions

(Note: The author had his share also in all papers co-finishing/revising.)

[JK1] First author, corresponding author.

Design of experiments, ellipsometry and thermal data acquisition and interpretation, paper preparation

[JK2] Second author.

FTIR and mass spectra data acquisition and interpretation

[JK3] First author, corresponding author.

Depositions, data acquisition and interpretation (without XPS), paper preparation

[JK4] Second author.

FTIR spectra acquisition and interpretation, elemental/volume ratios recalculation

[JK5] First author, corresponding author.

Design of experiments, theory, modelling, data processing and interpretation, paper preparation

[JK6] First author, corresponding author.

Design of experiments, depositions, mass spectra and OES data acquisition and interpretation, paper preparation

[JK7] First author, student (coauthor) supervisor.

Design of experiments and their operation (shared), data acquisition optimization, trapping effect detection, SAXS data processing (shared) and interpretation, paper preparation (shared)

[JK8] First author, corresponding author.

Target materials processing, experiments, FTIR and mass spectra data processing and interpretation, paper preparation

[JK9] First author, student (coauthor) supervisor.

Design of experiments, depositions, FTIR spectra and ellipsometry data acquisition and interpretation, release data processing, paper preparation, funding acquisition

[JK10] First author, corresponding author, student (coauthor) supervisor.

Design of experiments, FTIR spectra and ellipsometry data acquisition and interpretation, theory for data processing, data acquisition and interpretation, paper preparation, funding acquisition

[JK11] Corresponding author, student (first author) supervisor

Design of experiments, ellipsometry data interpretation, drafting of the model, paper preparation, funding acquisition

[JK12] Corresponding author, second author, students (first author, coauthor) supervisor

Design of experiments, FTIR spectra, ellipsometry and thermal stability data acquisition and interpretation, drug release kinetics data processing, paper preparation, funding acquisition

5. General references

[1] A. Fridman. *Plasma Chemistry*. Cambridge University Press, 1st edition, 2008. ISBN: 9780521847353.

[2] R. Hippler, H. Kersten, M. Schmidt, and K. H. Schoenbach, editors. *Low Temperature Plasmas: Fundamentals, Technologies and Techniques*. Wiley-VCH, 2nd edition, 2008. ISBN: 9783527406739.

[3] A. Anders. A structure zone diagram including plasma-based deposition and ion etching. *Thin Solid Films*, 518(15):4087–4090, 2010. ISSN: 0040-6090. DOI: 10.1016/j.tsf.2009.10.145.

[4] S. K. Nemani, R. K. Annavarapu, B. Mohammadian, A. Raiyan, J. Heil, M. A. Haque, A. Abdelaal, and H. Sojoudi. Surface Modification of Polymers: Methods and Applications. *Advanced Materials Interfaces*, 5(24):1801247, 2018. DOI: 10.1002/admi.201801247.

[5] R. L. Baxter, H. C. Baxter, G. A. Campbell, K. Grant, A. Jones, P. Richardson, and G. Whittaker. Quantitative analysis of residual protein contamination on reprocessed surgical instruments. *Journal of Hospital Infection*, 63(4):439–444, 2006. DOI: 10.1016/j.jhin.2006.03.011.

[6] M. Laroussi, S. Bekeschus, M. Keidar, A. Bogaerts, A. Fridman, X. Lu, K. Ostrikov, M. Hori, K. Stapelmann, V. Miller, S. Reuter, C. Laux, A. Mesbah, J. Walsh, C. Jiang, S. M. Thagard, H. Tanaka, D. Liu, D. Yan, and M. Yusupov. Low-Temperature Plasma for Biology, Hygiene, and Medicine: Perspective and Roadmap. *IEEE Transactions on Radiation and Plasma Medical Sciences*, 6(2):127–157, 2022. DOI: 10.1109/TRPMS.2021.3135118.

[7] J. R. Roth. *Industrial Plasma Engineering; Volume 2: Applications to Nonthermal Plasma Processing*. IOP Publishing, 1st edition, 2001. ISBN: 0750305444.

[8] J. E. Greene. Review Article: Tracing the recorded history of thin-film sputter deposition: From the 1800s to 2017. *Journal of Vacuum Science & Technology A*, 35(5):05C204, 2017. DOI: 10.1116/1.4998940.

[9] R. Harrop and P. J. Harrop. Friction of sputtered PTFE films. *Thin Solid Films*, 3(1969):109–117, 1968. DOI: 10.1016/0040-6090(69)90083-2.

[10] D. T. Morrison and T. Robertson. R.F sputtering of plastics. *Thin Solid Films*, 15:87–101, 1973. DOI: 10.1016/0040-6090(73)90207-1.

[11] H. Biederman, S. M. Ojha, and L. Holland. The properties of fluorocarbon films prepared by R.F. sputtering and plasma polymerization in inert and active gas. *Thin Solid Films*, 41:329–339, 1977. DOI: 10.1016/0040-6090(77)90319-4.

[12] H. Biederman. The properties of films prepared of PTFE and plasma polymerization by the rf sputtering of some freons. *Vacuum*, 31(7):285–289, 1981. DOI: 10.1016/S0042-207X(81)80498-8.

[13] H. Biederman, P. Bílková, J. Ježek, P. Hlídek, and D. Slavínská. RF magnetron sputtering of polymers. *Journal of Non Crystalline Solids*, 218:44–49, 1997. DOI: 10.1016/S0022-3093(97)00196-8.

[14] C. Rodriguez-Emmenegger, O. Kylián, M. Houska, E. Brynda, A. Artemenko, J. Kousal, A. Bologna Alles, and H. Biederman. Substrate-Independent Approach for the Generation of Functional Protein Resistant Surfaces. *Biomacromolecules*, 12:1058–1066, 2011. DOI: 10.1021/bm101406m.

[15] Q. Wei and R. Haag. Universal polymer coatings and their representative biomedical applications. *Materials Horizons*, 2:567–577, 2015. DOI: 10.1039/c5mh00089k.

[16] K. S. Siow, L. Britcher, S. Kumar, and H. J. Griesser. Plasma methods for the generation of chemically reactive surfaces for biomolecule immobilization and cell colonization - A review. *Plasma Processes and Polymers*, 3(6-7):392–418, 2006. DOI: 10.1002/ppap.200600021.

[17] F. Truica-Marasescu and M. R. Wertheimer. Nitrogen-Rich Plasma-Polymer Films for Biomedical Applications. *Plasma Processes and Polymers*, 5(1):44–57, 2008. DOI: 10.1002/ppap.200700077.

[18] K. Schröder, B. Finke, H. Jesswein, F. Lüthen, A. Diener, R. Ihrke, A. Ohl, K. Weltmann, J. Rychly, and J. B. Nebe. Similarities between Plasma Amino Functionalized PEEK and Titanium Surfaces Concerning Enhancement of Osteoblast Cell Adhesion. *ournal of Adhesion Science and Technology*, 24(5):905–923, 2010. DOI: 10.1163/016942409X12598231567989.

[19] M. M. M. Bilek, D. V. Bax, A. Kondyurin, Y. Yin, N. J. Nosworthy, K. Fisher, A. Waterhouse, A. S. Weiss, C. G. dos Remedios, and D. R. McKenzie. Free radical functionalization of surfaces to prevent adverse responses to biomedical devices. *Proceedings of*

the National Academy of Sciences, 108(35):14405–14410, 2011. DOI: 10.1073/pnas.1103277108.

[20] D. Hegemann, B. Hanselmann, S. Guimond, G. Fortunato, M.-N. Giraud, and A. G. Guex. Considering the degradation effects of amino-functional plasma polymer coatings for biomedical application. *Surface & Coatings Technology*, 255:90–95, 2014. DOI: 10.1016/j.surfcoat.2014.01.054.

[21] A. Fahmy, T. A. Mohamed, and J. F. Friedrich. XPS and IR studies of plasma polymers layer deposited from allylamine with addition of ammonia. *Applied Surface Science*, 458:1006–1017, 2018. DOI: 10.1016/j.apsusc.2018.07.160.

[22] J. Ibrahim, S. A. Al-Bataineh, A. Michelmore, and J. D. Whittle. Atmospheric Pressure Dielectric Barrier Discharges for the Deposition of Organic Plasma Polymer Coatings for Biomedical Application. *Plasma Chemistry and Plasma Processing*, 41:47–83, 2021. DOI: 10.1007/s11090-020-10135-6.

[23] N. B. Singh, editor. *Nanocomposites*. Jenny Stanford Publishing, New York, 1st edition, 2022. ISBN: 9781003314479.

[24] J. Peng and Q. Cheng. High-Performance Nanocomposites Inspired by Nature. *Advanced Materials*, 29(45):1702959, 2017. DOI: 10.1002/adma.201702959.

[25] I. U. Unalan, G. Cerri, E. Marcuzzo, C. A. Cozzolino, and S. Farris. Nanocomposite films and coatings using inorganic nanobuilding blocks (NBB): current applications and future opportunities in the food packaging sector. *RSC Advances*, 4(56):29393–29428, 2014. DOI: 10.1039/C4RA01778A.

[26] M. Faraday. X. The Bakerian Lecture. — Experimental relations of gold (and other metals) to light. *Philosophical Transactions of the Royal Society of London*, 147:145–181, 1857. DOI: 10.1098/rstl.1857.0011.

[27] C. Dhand, N. Dwivedi, X. J. Loh, A. N. J. Ying, N. K. Verma, R. W. Beuerman, R. Lakshminarayanan, and S. Ramakrishna. Methods and strategies for the synthesis of diverse nanoparticles and their applications: a comprehensive overview. *RSC Advances*, 5(127):105003–105037, 2015. DOI: 10.1039/C5RA19388E.

[28] C. Binns. Nanoclusters deposited on surfaces. *Surface Science Reports*, 44(1-2):1–49, 2001. DOI: 10.1016/S0167-5729(01)00015-2.

[29] H. Haberland, M. Karrais, and M. Mall. A new type of cluster and cluster ion source. *Zeitschrift für Physik D Atoms, Molecules and Clusters*, 20(1):413–415, 1991. DOI: 10.1007/BF01544025.

[30] R. Hippler, M. Cada, V. Stranak, Z. Hubicka, and C. A. Helm. Pressure dependence of Ar_2^+ $ArTi^+$ and Ti_2^+ dimer formation in a magnetron sputtering discharge. *Journal of Physics D: Applied Physics*, 50(44):445205, 2017. DOI: 10.1088/1361-6463/aa8b9a.

[31] Y. Huttel, editor. *Gas-Phase Synthesis of Nanoparticles*. Wiley-VCH, 1st edition, 2017. ISBN: 9783527340606.

[32] A. Marek, J. Valter, S. Kadlec, and J. Vyskočil. Gas aggregation nanocluster source — Reactive sputter deposition of copper and titanium nanoclusters. *Surface & Coatings Technology*, 205:S573–S576, 2011. DOI: 10.1016/j.surfcoat.2010.12.027.

[33] T. Peter, O. Polonskyi, B. Gojdka, A. M. Ahadi, T. Strunskus, V. Zaporojtchenko, H. Biederman, and F. Faupel. Influence of reactive gas admixture on transition metal cluster nucleation in a gas aggregation cluster source. *Journal of Applied Physics*, 112:114321, 2012. DOI: 10.1063/1.4768528.

[34] O. Polonskyi, T. Peter, A. M. Ahadi, A. Hinz, T. Strunskus, V. Zaporojtchenko, H. Biederman, and F. Faupel. Huge increase in gas phase nanoparticle generation by pulsed direct current sputtering in a reactive gas admixture. *Applied Physics Letters*, 103:033118, 2013. DOI: 10.1063/1.4816036.

[35] G. Krishnan, S. D. Graaf, G. H. ten Brink, P. O. Å. Persson, B. J. Kooi, and G. Palasantzas. Strategies to initiate and control the nucleation behavior of bimetallic nanoparticles. *Nanoscale*, 9:8149–8156, 2017. DOI: 10.1039/c7nr00916j.

[36] B. M. Smirnov, I. Shyjumon, and R. Hippler. Flow of nanosize cluster-containing plasma in a magnetron discharge. *Physical Review E*, 75:066402, 2007. DOI: 10.1103/PhysRevE.75.066402.

[37] M. Ganeva, A. V. Pipa, B. M. Smirnov, P. V. Kashtanov, and R. Hippler. Velocity distribution of mass-selected nano-size cluster ions. *Plasma Sources Science and Technology*, 22(4):045011, 2013. DOI: 10.1088/0963-0252/22/4/045011.

[38] P. Solař, J. Kousal, J. Hanuš, K. Škorvánková, A. Kuzminova, and O. Kylián. Mechanical time - of - flight filter based on slotted disks and helical rotor for measurement of velocities of nanoparticles. *Scientific Reports*, 11:6415, 2021. DOI: 10.1038/s41598-021-85533-7.

[39] J. Hanuš, M. Vaidulych, O. Kylián, A. Choukourov, J. Kousal, I. Khalakhan, M. Cieslar, P. Solař, and H. Biederman. Fabrication of Ni@Ti core–shell nanoparticles by modified gas aggregation source. *Journal of Physics D: Applied Physics*, 50(47):475307, 2017. DOI: 10.1088/1361-6463/aa8f25.

[40] L. Zhang, J. Shao, and X. Chen. Numerical simulation of nanocluster motion through a DC magnetron nanocluster source. *Vaccum*, 128:137–145, 2016. DOI: 10.1016/j.vacuum.2016.03.011.

[41] R. Rudd, A. Obrusník, P. Zikán, C. Hall, P. Murphy, D. Evans, and E. Charrault. Plasma gas aggregation cluster source: Influence of gas inlet configuration and total surface area on the heterogeneous aggregation of silicon clusters. *Surface & Coatings Technology*, 364:1–6, 2019. DOI: 10.1016/j.surfcoat.2019.02.074.

[42] G. Sanzone, J. Yin, K. Cooke, H. Sun, and P. Lievens. Impact of the gas dynamics on the cluster flux in a magnetron cluster-source: Influence of the chamber shape and gas- inlet position. *Review of Scientific Instruments*, 033901(92):033901, 2021. DOI: 10.1063/5.0028854.

[43] S. Ali-Ogly, J. Kousal, D. Nikitin, P. Pleskunov, J. Hanuš, A. Choukourov, and H. Biederman. Computational fluid dynamics predicts the nanoparticle transport in gas aggregation cluster sources. *Journal of Physics D: Applied Physics*, 55(44):445203, 2022. DOI: 10.1088/1361-6463/ac8c4e.

[44] J. Blažek, P. Bartoš, R. Basner, and H. Kersten. Distribution of charge on clusters in a magnetron discharge. In *Proceedings of 30th ICPIG*, B5–322, 2011.

[45] A. Melzer. Mode spectra of thermally excited two-dimensional dust Coulomb clusters. *Physical Review E*, 67:016411, 2003. DOI: 10.1103/PhysRevE.67.016411.

[46] M. Bonitz. *Complex Plasmas: Scientific Challenges and Technological Opportunities*. M. Bonitz, J. Lopez, K. Becker, and H. Thomsen, editors. Springer Cham, 1st edition, 2014. ISBN: 9783319054360. DOI: 10.1007/978-3-319-05437-7.

[47] H. R. Maurer, V. Schneider, M. Wolter, R. Basner, T. Trottenberg, and H. Kersten. Microparticles as Plasma Diagnostic Tools. *Contributions to Plasma Physics*, 51(2-3):218–227, 2011. DOI: 10.1002/ctpp.201000091.

[48] A. Bouchoule and L. Boufendi. Particulate formation and dusty plasma behaviour in argon–silane RF discharge. *Plasma Sources Science and Technology*, 2(3):204, 1993. DOI: 10.1088/0963-0252/2/3/011.

[49] E. Kovačević, I. Stefanović, J. Berndt, and J. Winter. Infrared fingerprints and periodic formation of nanoparticles in Ar/C_2H_2 plasmas. *Journal of Applied Physics*, 93(5):2924–2930, 2003. DOI: 10.1063/1.1541118.

[50] M. A. Koten, S. A. Voeller, M. M. Patterson, and J. E. Shield. In situ measurements of plasma properties during gas-condensation of Cu nanoparticles. *Journal of Applied Physics*, 119:114306, 2016. DOI: 10.1063/1.4943630.

[51] A. Shelemin, O. Kylián, J. Hanuš, A. Choukourov, I. Melnichuk, A. Serov, D. Slavínská, and H. Biederman. Preparation of metal oxide nanoparticles by gas aggregation cluster source. 120:162–169, 2015. DOI: 10.1016/j.vacuum.2015.07.008.

[52] J. Musil, P. Baroch, J. Vlček, K. H. Nam, and J. G. Han. Reactive magnetron sputtering of thin films: present status and trends. *Thin Solid Films*, 475:208–218, 2005. DOI: 10.1016/j.tsf.2004.07.041.

[53] F. F. Chen. *Lecture Notes on Langmuir Probe Diagnostics*. IEEE-ICOPS, 2003.

[54] C. Arnas, T. Guidez, A. Chami, J. H. Mun, and L. Couedel. Forces applied to nanoparticles in magnetron discharges and the resulting size segregation. *Physics of Plasmas*, 29:073703, 2022. DOI: 10.1063/5.0095103.

[55] I. Barke, H. Hartmann, D. Rupp, L. Flückiger, M. Sauppe, M. Adolph, S. Schorb, C. Bostedt, R. Treusch, C. Peltz, S. Bartling, T. Fennel, K.-H. Meiwes-Broer, and T. Möller. The 3D-architecture of individual free silver nanoparticles captured by X-ray scattering. *Nature Communications*, 6:6187, 2015. DOI: 10.1038/ncomms7187.

[56] A. Shelemin, P. Pleskunov, J. Kousal, J. Drewes, J. Hanuš, S. Ali-Ogly, D. Nikitin, P. Solař, J. Kratochvíl, M. Vaidulych, M. Schwartzkopf, O. Kylián, O. Polonskyi, T. Strunskus, F. Faupel, S. V. Roth, H. Biederman, and A. Choukourov. Nucleation and Growth of Magnetron-Sputtered

Ag Nanoparticles as Witnessed by Time-Resolved Small Angle X-Ray Scattering. *Particle & Particle Systems Characterization*, 37(2):1900436, 2020. DOI: 10.1002/ppsc.201900436.

[57] D. Nikitin, J. Hanuš, S. Ali-Ogly, O. Polonskyi, J. Drewes, F. Faupel, H. Biederman, and A. Choukourov. The evolution of Ag nanoparticles inside a gas aggregation cluster source. 16(10):e1900079, 2019. DOI: 10.1002/ppap.201900079.

[58] J. Drewes, S. Ali-Ogly, T. Strunskus, O. Polonskyi, H. Biederman, F. Faupel, and A. Vahl. Impact of argon flow and pressure on the trapping behavior of nanoparticles inside a gas aggregation source. *Plasma Processes and Polymers*, 19:e2100125, 2022. DOI: 10.1002/ppap.202100125.

[59] J. Drewes, S. Rehders, T. Strunskus, H. Kersten, F. Faupel, and A. Vahl. In Situ Laser Light Scattering for Temporally and Locally Resolved Studies on Nanoparticle Trapping in a Gas Aggregation Source. *Particle & Particle Systems Characterization*, 39(11):2200112, 2022. DOI: 10.1002/ppsc.202200112.

[60] J. König and G. Helwig. Über dünne aus Kohlenwasserstoffen durch Elektronen - oder Ionenbeschuß gebildete Schichten. *Zeitschrift für Physik*, 129:491–503, 1951. DOI: 10.1007/BF01330048.

[61] A. Bradley and J. P. Hammes. Electrical Properties of Thin Organic Films. *Journal of The Electrochemical Society*, 110(1):15–22, 1963. DOI: 10.1149/1.2425663.

[62] M. White. Vacuum evaporation of Polythene. *Vacuum*, 15(9):449–450, 1965. DOI: 10.1016/0042-207X(65)92111-1.

[63] P. P. Luff and M. White. Thermal degradation of polyethylene and polytetrafluoroethylene during vacuum evaporation. *Vacuum*, 18(8):437–440, 1968. DOI: 10.1016/0042-207X(68)90336-9.

[64] T. C. Nason, J. A. Moore, and T.-M. Lu. Deposition of amorphous fluoropolymer thin films by thermolysis of Teflon amorphous fluoropolymer. *Applied Physics Letters*, 60(15):1866–1868, 1992. DOI: 10.1063/1.107163.

[65] H. Usui, I. Yamada, and T. Takagi. Anthracene and polyethylene thin film depositions by ionized cluster beam. *Journal of Vacuum Science & Technology A*, 4(1):52–60, 1986. DOI: 10.1116/1.573497.

[66] H. Usui, H. Koshikawa, and K. Tanaka. Effect of substrate temperature on the deposition of polytetrafluoroethylene by an ionization-assisted evaporation method. *Journal of Vacuum Science & Technology A*, 13(5):2318–2324, 1995. DOI: 10.1116/1.579515.

[67] G. Maggioni, S. Carturan, V. Rigato, and U. Pieri. Effects of the ion–solid interaction in glow discharge vapour deposition polymerization of pyromellitic dianhydride. *Nuclear Instruments and Methods in Physics Research B*, 166-167:737–742, 2000. DOI: 10.1016/S0168-583X(99)01063-0.

[68] G. Maggioni, S. Carturan, V. Rigato, and G. Della Mea. Glow discharge vapour deposition polymerisation of polyimide thin coatings. *Surface and Coatings Technology*, 142-144:156–162, 2001. DOI: 10.1016/S0257-8972(01)01093-3.

[69] A. Barranco, F. Aparicio, A. Yanguas-Gil, P. Groening, J. Cotrino, and A. R. Gonzáles-Elipe. Optically Active Thin Films Deposited by Plasma Polymerization of Dye Molecules. *Chemical Vapor Deposition*, 13:319–325, 2007. DOI: 10.1002/cvde.200606552.

[70] I. Blaszczyk-Lezak, F. J. Aparicio, A. Borrás, A. Barranco, A. Alvárez-Herrero, M. Fernández-Rodríguez, and A. R. Gonzáles-Elipe. Optically Active Luminescent Perylene Thin Films Deposited by Plasma Polymerization. *Journal of Physical Chemistry C*, 113:431–438, 2009. DOI: 10.1021/jp807634j.

[71] I. Kholodkov, H. Biederman, D. Slavínská, A. Choukourov, and A. Trchová. Plasma polymers prepared by RF sputtering of polyethylene. *Vacuum*, 70:505–509, 2003. DOI: 10.1016/S0042-207X(02)00702-9.

[72] A. Choukourov, J. Hanuš, J. Kousal, A. Grinevich, Y. Pihosh, D. Slavínská, and H. Biederman. Thin polymer films from polyimide vacuum thermal degradation with and without a glow discharge. *Vacuum*, 80:923–929, 2006. DOI: 10.1016/j.vacuum.2005.12.012.

[73] A. Choukourov, I. Gordeev, D. Arzhakov, A. Artemenko, J. Kousal, O. Kylián, D. Slavínská, and H. Biederman. Does cross-link density of PEO-like plasma polymers influence their resistance to adsorption of fibrinogen? *Plasma Processes and Polymers*, 9(1):48–58, 2012. DOI: 10.1002/ppap.201100122.

[74] A. Choukourov, I. Gordeev, J. Ponti, C. Uboldi, I. Melnichuk, M. Vaidulych, J. Kousal, D. Nikitin, L. Hanyková, I. Krakovský, D. Slavínská, and H. Biederman. Microphase-Separated PE/PEO Thin Films Prepared by Plasma-Assisted Vapor Phase Deposition. *ACS Applied Materials and Interfaces*, 8(12):8201–8212, 2016. DOI: 10.1021/acsami.5b12382.

[75] X. Huang and C. S. Brazel. On the importance and mechanisms of burst release in matrix-controlled drug delivery systems. *Journal of Controlled Release*, 73(2-3):121–136, 2001. DOI: 10.1016/S0168-3659(01)00248-6.

[76] H. Yasuda. *Plasma Polymerization*. Academic Press, 1st edition, 1985. ISBN: 9780323139458.

[77] D. Thiry, S. Konstantinidis, J. Cornil, and R. Snyders. Plasma diagnostics for the low-pressure plasma polymerization process: A critical review. *Thin Solid Films*, 606:19–44, 2016. DOI: 10.1016/j.tsf.2016.02.058.

[78] K. Rügner, R. Reuter, D. Ellerweg, T. de los Arcos, A. von Keudell, and J. Benedikt. Insight into the Reaction Scheme of SiO_2 Film Deposition at Atmospheric Pressure. *Plasma Processes and Polymers*, 10(2):1061–1073, 2013. DOI: 10.1002/ppap.201300059.

[79] D. Loffhagen, M. M. Becker, A. K. Czerny, J. Philipp, and C.-P. Klages. Impact of hexamethyldisiloxane admixtures on the discharge characteristics of a dielectric barrier discharge in argon for thin film deposition. 58(5):337–352, 2018. DOI: 10.1002/ctpp.201700060.

[80] D. Hegemann, E. Bülbül, B. Hanselmann, U. Schütz, M. Amberg, and S. Gaiser. Plasma polymerization of hexamethyldisiloxane: Revisited. *Plasma Processes and Polymers*, 18(2):e2000176, 2021. DOI: 10.1002/ppap.202000176.

[81] S. Ligot, F. Renaux, L. Denis, D. Cossement, N. Nuns, P. Dubois, and R. Snyders. Experimental study of the plasma polymerization of ethyl lactate. *Plasma Processes and Polymers*, 10(11):999–1009, 2013. DOI: 10.1002/ppap.201300025.

[82] M. Laurent, E. Desjardins, M. Meichelboeck, N. Naudé, L. Stafford, N. Gherardi, and G. Laroche. Characterization of argon dielectric barrier discharges applied to ethyl lactate plasma polymerization. *Journal of Physics D: Applied Physics*, 50:475205, 2017. DOI: 10.1088/1361-6463/aa916d.

6. Full texts of selected publications

(in the full-length version of this thesis only)